ACS APPLIED MATERIALS & INTERFACES

Research Article

www.acsami.org

Omniphobic Low Moisture Permeation Transparent Polyacrylate/Silica Nanocomposite

Sheng-Hao Hsu,[†] Yuan-Ling Chang,[‡] Yu-Chieh Tu,[‡] Chieh-Ming Tsai,[‡] and Wei-Fang Su*[,†,‡]

[†]Institute of Polymer Science and Engineering and [‡]Department of Materials Science and Engineering, National Taiwan University, Taipei 10617, Taiwan

ABSTRACT: We report the development of low moisture permeation and transparent dense polyacrylate/silica nanocomposite material that can exhibit both superhydrophobic and oleophobic (omniphobic) properties. The material was prepared by a three-step process. The first step involved the preparation of UV polymerizable solventless hybrid resin and the fabrication of nanocomposite. The hybrid resin consisted of a mixture of acrylate monomer, initiator, and acrylate-modified different size silica nanoparticles. The second step was to roughen the surface of the nanocomposite with unique nanotexture by oxygen plasma. In the third step, we applied a low surface tension fluoro monolayer on the treated surface. The nanocomposite exhibits desired superhydrophobicity and oleophobicity with a water contact angle of 158.2° and *n*-1-octadecene contact angle of 128.5°, respectively; low moisture permeation of 1.44 g·mm/m^2·day; and good transparency (greater than 82% at 450−800 nm for ∼60 μm film). The material has potential applications in optoelectronic encapsulation, self-cleaning coating, etc.

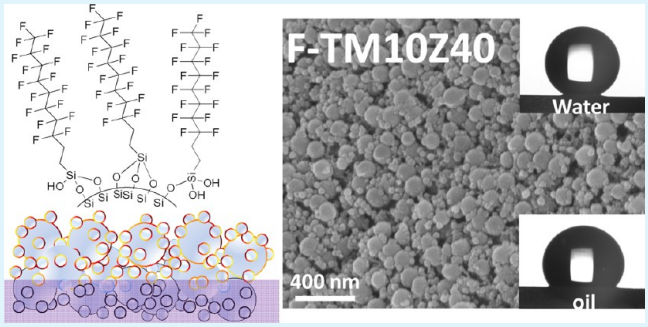

KEYWORDS: *superhydrophobic, oleophobic, omniphobic, nanocomposite, nanotexture, plasma*

1. INTRODUCTION

Many natural surfaces, including lotus leaves, cicada wings, and water strider legs, exhibit superhydrophobicity with an apparent water contact angle above 150°.[1−3] These remarkable water-repellent properties have stimulated numerous studies on their mechanisms and potential applications.[4−12] Two key factors, surface roughness and surface energy, determine the liquid-repellent property on the surface. The Cassie−Baxter model and the Wenzel model are commonly employed to discuss the relation between roughness and liquid repellency. The Cassie−Baxter model suggests that the hydrophobicity of the roughened surface results from the air pockets trapped under the liquid droplet and thus leads to high contact angles and small contact angle hysteresis.[13] On the contrary, the contacted state below the droplet postulated by the Wenzel model results in lower contact angles and larger hysteresis.[14] Recently, Tuteja et al. suggested a metastable Cassie−Baxter model to explain the unexpected superhydrophobicity on the surface of the lotus leaf. They showed the possibility that an omniphobic surface could be achieved by fabricating the re-entrant structure on the surface without using extremely low surface tension materials.[5,6]

Various techniques have been developed to fabricate the artificial nonwetting surfaces. Tuteja et al. prepared omniphobic surfaces by electrospinning blends of fluorodecyl polyhedral oligomeric silsesquioxane (POSS) and poly(methyl methacrylate) (PMMA).[5,6] Tsougeni et al. developed superhydrophobic surfaces by O_2 plasma etching and then followed by C_4F_8 plasma deposition on the polymer substrate.[15] Other methods involved sol−gel self-assembly, 3-D diffuser lithography, wet chemical etching, composite blending, dip-coating, and plasma process.[16−24] However, all of these techniques created high surface roughness by introducing pores, special patterns, or texture onto the surface of the material, which may decrease the barrier properties and/or transparency of the coatings.

In this study, the issues have been resolved by developing a dense omniphobic durable nanocomposite with high transparency and low moisture permeation. We achieved, from our previous work, that a transparent hydrophobic durable low moisture permeation poly(fluoroimide acrylate)/SiO_2 nanocomposite can be obtained by increasing the surface roughness of the coating through nanosized SiO_2 aggregation in a polymer matrix.[25] Here, we further the technology to develop a novel superhydrophobic and oleophobic transparent nanocomposite dense film by a combination of unique nanotexture rough surface plus low surface tension coating using a three-step process. The results are summarized and discussed in the following sections.

2. EXPERIMENTAL SECTION

2.1. Materials. The following chemicals were used as received without further purification: colloidal solution of ∼25 nm spherical silica (20−30 nm, MA-S-TM, 40 wt % solid content, Nissan Chemical Industries, Ltd.), colloidal solution of ∼100 nm spherical silica (70−

Received: October 24, 2012
Accepted: March 18, 2013
Published: March 18, 2013

100 nm ST-ZL, 40 wt % solid content, Nissan Chemical Industries, Ltd.), 3-(trimethoxysilyl) propyl methacrylate (MPS, 98%, Acros Organics), tricyclodecane dimethanol diacrylate (TCDDA, Sartomer Co., Inc.), 1-hydroxycyclohexyl-phenyl-ketone (Irgacure 184, Ciba Inc.), 1*H*,1*H*,2*H*,2*H*-perfluorodecyl trimethoxysilane (PFDTMES, 99%, Gelest Inc.), acetic acid (99.5%, Acros Organics), and ethanol (95% and 99.5%, Acros Organics). The chemical structures of major chemicals TCDDA, MPS, and PFDTMES for the preparation of nanocomposites are illustrated in Figure 1.

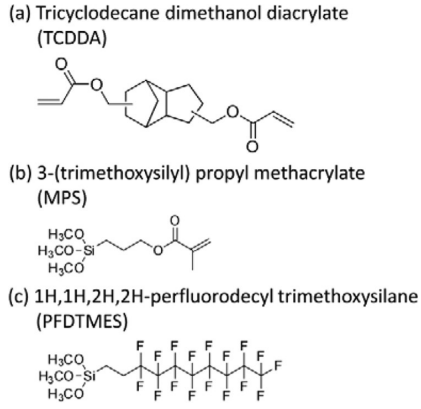

Figure 1. Chemical structures of (a) TCDDA, (b) MPS, and (c) PFDTMES.

2.2. Preparation of MPS-Modified Silica Colloidal Solutions. For the preparation of MPS-modified ~25 nm silica nanoparticles (named M-silica), 20.0 g of MA-S-TM SiO_2 colloidal solution (40 wt %) was mixed with 20.0 g of ethanol (95%) and stirred for 10 min. An amount of 2.0 g of MPS was added into the mixture and stirred at 50 °C for 24 h. For the preparation of MPS-modified ~100 nm SiO_2 nanoparticles (named Z-silica), 20.0 g of ST-ZL silica colloidal solution (40 wt %) was mixed with 20.0 g of ethanol (95%) and stirred for 10 min. Then, 0.8 g of MPS was added into the mixture and stirred at 50 °C for 24 h. The solid content of MPS-modified silica colloidal solutions was measured by thermogravimetric analysis before use.

2.3. Preparation of Photocurable Nanocomposite Resins. The surface-modified silica colloidal solutions with varied ratios of M-silica to Z-silica were added to a mixture of TCDDA and photoinitiator (Irgacure 184), respectively, and stirred for 30 min first, and then the solvent was removed by vacuum at 10^{-3} mmHg for 1 h to obtain a series of nanocomposite resins, and the compositions are listed in Table 1. The weight of MPS-modified silica nanoparticles accounted for 50 wt % in each resin formulation. The denotation of TMXXZYY was used to describe different samples and compositions of nanocomposite resins. The first letter T indicated the acrylate resin of TCDDA, the second letter M the M-silica of ~25 nm diameter, and the letter Z the ~100 nm Z-silica. The letters "XX" and "YY" indicated the weight percent of M-silica and Z-silica in the nanocomposite resin, respectively.

Table 1. Compositions of Various UV Curable Nanocomposite Resins

	composition (wt %)			
sample name	TCDDA resin	M-silica ~25 nm	Z-silica ~100 nm	Irgacure 184 photoinitiator
TM00Z50	49.02	0	49.02	1.96
TM10Z40	49.02	9.80	39.22	1.96
TM25Z25	49.02	24.51	24.51	1.96
TM40Z10	49.02	39.22	9.80	1.96
TM50Z00	49.02	49.02	0	1.96

2.4. Preparation of Nanocomposite Samples. For evaluating the absorption property of the nanocomposite, the ~60 μm film thickness of the nanocomposite sample was prepared by casting the resin on the glass substrate, using two strips of 3M 810D Scotch tape as spacers. The resin was isolated from air by placing polyethylene terephthalate (PET) film on top of the resin, and the resin was cured through the PET film by a high-powered UV-lamp box (935 W/m^2, OPAS XLite 400Q) with one-minute exposure at a distance of 20 cm. The film thickness was measured by a thickness gauge (ABS Digimatic Indicator Series 543, Mitsutoyo).

For evaluating the property of water vapor transmission rate (WVTR) of nanocomposite films, the ~150 μm free-standing film was prepared by casting the resin on a glass slide, and the thickness of the uncured coating was controlled by 3M VHB tape as spacers. The resin was cured by the same UV-lamp box with one-minute exposure at a distance of 20 cm. The thickness of the cured samples was determined by an electronic thickness gauge (Teclock USG-10).

For determining the water absorption property of the nanocompsite, the disk sample of 5 mm (diameter) × 2 mm (thick) was prepared by casting the nanocomposite resin in a stainless steel mold. The resin was cured by the same UV-lamp box for one minute from the top side and bottom side, respectively.

2.5. Preparation of Oxygen Plasma Treated Nanocomposite Samples. The photocured nanocomposite sample was put into the chamber of the plasma cleaner (Harrick Plasma) and treated by oxygen plasma for ten minutes. The oxygen pressure of 6×10^{-1} mmHg and power of 18 W were adopted. For the disk sample, the top side and bottom side of the sample were treated by the same plasma condition, respectively. The samples treated by oxygen plasma were named as OP-TMXXZYY series where OP indicated oxygen plasma treatment.

2.6. Preparation of Dip-Coating Solution. An amount of 3 mL of distilled water was added into 100 mL of ethanol (99.5 vol %) to make an ethanol solution. Then, an appropriate amount of acetic acid was added into the ethanol solution to adjust its pH value to 2.8. An amount of 2 mL of 1*H*,1*H*,2*H*,2*H*-perfluorodecyl trimethoxysilane (PFDTMES) was then added into the acidic ethanol solution and stirred for 20 min at 25 °C to hydrolyze the PFDTMES. A dip-coating fluorosilane solution of PFDTMES was obtained.

2.7. Preparation of Fluorosilane-Coated Nanocomposite Samples. The dip-coating process was executed by a KSV Dip Coater. The oxygen plasma treated sample was dipped into the dip-coating solution at a rate of 50 mm/min. After 15 min, the sample was withdrawn at a rate of 15 mm/min, and then the coated samples were heated at 80 °C for 1 h. The fluorosilane-coated samples were labeled as F-TMXXZYY series where F indicates the samples were coated by fluorosilane.

2.8. Characterization of the Nanocomposite. The ultrathin TEM nanocomposite film was prepared using a Leika EM UC6 ultramicrotome machine at room temperature. A Drukker ultra-microtome knife with cutting edge of 45° was used to obtain an ~80 nm film sample that was then placed on a 200-mesh copper grid. The sample was studied by using a JEOL JEM 1230 electron microscope with a LaB6 filament, operating at an accelerating voltage of 100 kV.

The surface morphology of TM00Z50, OP-TM00Z50, and F-TMXXZYY series films coated with platinum was studied by a JEOL JSM-6700F field emission scanning electron microscope at an accelerating voltage of 10 kV.

The surface roughness of the samples was measured by a Veeco Dektak 6M stylus profiler (Alpha stepper). The stylus force was 3 mg, and the scanning speed was 0.1 mm/s. Ten lines of 2 mm length for each sample were measured, and then the average and standard deviation of the roughness were calculated.

The chemical compositions of TM10Z40, OP-TM10Z40, and F-TM10Z40 surfaces were detected by a PHI VersaProbe X-ray photoelectron spectroscopy (XPS) in an ultrahigh vacuum chamber (1×10^{-6} mmHg). The energy pass was 58.7 eV, and the energy step was set at 0.5 eV.

The water and oil contact angles of the nanocomposite film were determined by a contact angle analyzer (Sindatek model 100SB).

Distilled water and *n*-1-octadecene (surface tension is 27.6 mN/m) were used for the water and oil contact angle measurement, respectively. The advancing and receding angles were measured during the period of continuously adding and withdrawing liquid to the droplets by a 0.4 mm diameter needle. Ten measurements were performed on each sample, and then the average and standard deviation of the angles were calculated.

The visible light transmittance of ~60 μm nanocomposite film was measured by an UV−vis spectrometer (Perkin-Elmer Lambda 35). The film was casted on a 1 mm glass substrate, and the same substrate was used as the reference in the measurement.

The water absorption of the nanocomposites was determined by the weight difference between before and after reflux in boiling water. The disk sample was weighted first after being dried at 100 °C overnight and then cooled to room temperature in a desiccator. The dried sample was immersed in 100 °C distilled water for 24 h, and then the sample was cooled to room temperature. The sample was weighed again after wiping off the water on its surface.

The WVTR of nanocomposite films was determined by using permeability cups (S-1003, Sheen Instruments) in a temperature- and humidity-controlled environmental chamber (Terchy HRM-80FA, Taichy Tech. Co., Taiwan). The film thickness is ~150 μm, and the test area is 10 cm^2. The test method followed the ASTM E96 method. We have included the film thickness in the calculation to obtain specific permeability.

3. RESULTS AND DISCUSSION

3.1. Compositions of the Nanocomposites. Our previous study[25] indicated that the surface roughness and the water contact angle were increased with the formation of nanosize aggregation in the nanocomposite obtained from hydrophobic poly(fluoroimide acrylate)-co-poly(neopentyl glycol diacrylate) and the acrylated silane (MPS) modified ~25 nm silica nanoparticle (named M-silica in this study). The fluoro polymer was laid on the surface of the nanocomposite without texture, so only superhydrophoblic property was observed. To achieve omniphobic property, we wanted to create nanotexture by exposing the silica nanoparticles on the surface of the nanocomposite by oxygen plasma, but it was too chemically stable to be etched. Here, we replaced the poly(fluoroimide acrylate)-co-poly(neopentyl glycol diacrylate) by poly(tricyclodecane dimethanol diacrylate). We measured the water permeation properties of this polyacrylate. It exhibited low water absorption (1.06 wt %) and low WVTR (12.02 g·mm/m^2·day) due to the hydrophobicity and ring structure of tricyclodecane. The polyacrylate contains C−C, C−H single bonds which are susceptible to oxygen plasma destruction. Thus, the monomer of this poly(tricyclodecane dimethanol diacrylate) (TCDDA) was used as an organic matrix in this new nanocomposite resin. To further increase the roughness of the nanocomposite after oxygen plasma treatment, the small size ~25 nm M-silica was mixed with the large-sized MPS-modified silica nanoparticle (Z-silica, ~100 nm). The optimal mixing ratio of M-silica/Z-silica was investigated by varying the amount from 1:4 to 4:1. The total silica content was fixed at 50 wt % in nanocomposites for good chemical, physical, and optical properties according to our previous study.[25,26] The TM10Z40 series nanocomposites showed the best overall properties which contained a 10:40 weight ratio of M-silica and Z-silica. These results are discussed below.

3.2. Surface Analysis of the Nanocomposites. For the better SEM image contrast between the organic matrix and silica, we selected the nanocomposite sample containing only large size silica (TM00Z50 contains 50 wt % Z-silica) to illustrate the effect of oxygen treatment on the surface morphology of the nanocomposite. Most of the silica nanoparticles were buried under the polyacrylate matrix before the oxygen plasma treatment as shown in Figure 2(a). After the

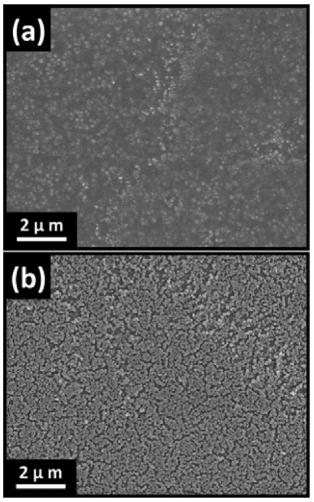

Figure 2. SEM top-view images of TM00Z50 nanocomposite film (a) before and (b) after oxygen plasma treatment.

plasma treatment, silica nanoparticles on the surface were exposed to air as indicated in Figure 2(b). Thus, the results of a SEM study confirmed the success of surface resin removal by oxygen plasma treatment. Then, the surface-roughened nanocomposite (TMXXZYY) was coated with fluorosilane of PFDTMES to obtain an omniphobic nanocomposite of F-TMXXZYY. Figure 3 shows the schematic illustration of the

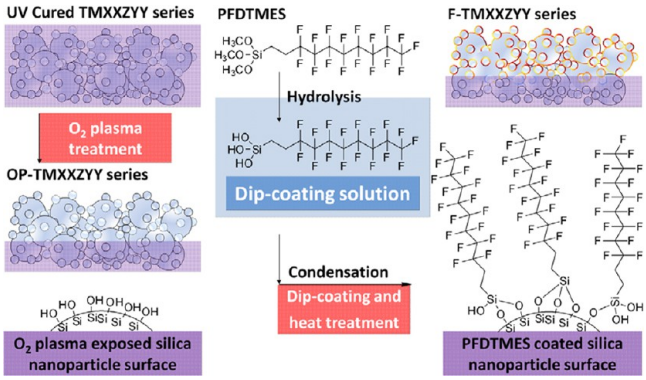

Figure 3. Schematic illustration of the preparation of F-TMXXZYY series nanocomposites.

preparation of an omniphobic nanocomposite. A monolayer of long alkyl chain fluoro coating was formed on the surface of the nanocomposite by the hydrolysis of SiO−CH_3 of PFDTMES and then the condensation between hydrolyzed fluorosilane and the Si−OH of silica.[27,28]

The chemical compositions on the surface of the nanocomposite were analyzed by XPS after each stage of preparation as shown in Figure 4. The samples with the best omniphobic performance (TM10Z40 series nanocomposites) were chosen for the surface chemistry analysis. As compared with the spectrum of pristine nanocomposite film of TM10Z40, the oxygen plasma treated film (OP-TM10Z40) exhibited a significant increase in the O 1s peak at 533 eV. The increased signal of O 1s may come from both the oxidation of the surface

dx.doi.org/10.1021/am302446t | ACS Appl. Mater. Interfaces 2013, 5, 2991−2998

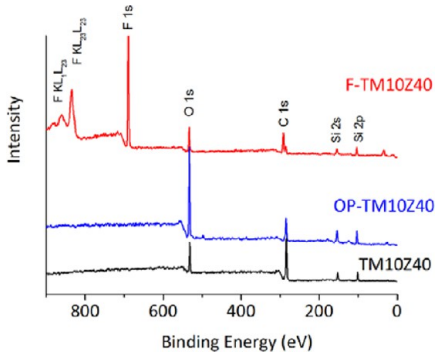

Figure 4. XPS spectra of the surface of the nanocomposite after different stages of preparation: pristine film (TM10Z40), oxygen plasma treated film (OP-TM10Z40), and fluorosilane-coated OP-TM10Z40 (F-TM10Z40).

and the exposed SiO_2. After the dip-coating, the peaks of F KL_1L_{23} (862 eV), F $KL_{23}L_{23}$ (834 eV), and F 1s (688 eV) became visible as shown in the sample of F-TM10Z40. They were from the CF_2 and CF_3 groups of PFDTMES. The results confirmed the oxygen plasma-treated surface was successfully covered by fluorosilane of PFDTMES via dip-coating.

We used a surface profiler instead of an atomic force microscope to measure the surface roughness of a large area of nanocomposites. The effect of silica compositions on the surface roughness of a nanocomposite after each stage of treatment was illustrated in Figure 5. All of the pristine

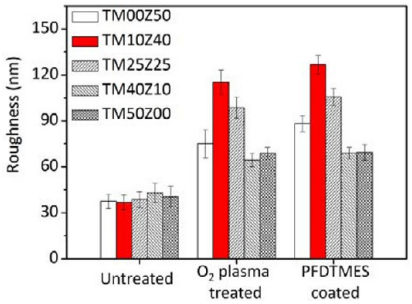

Figure 5. Average surface roughness (R_a) of various nanocomposites (TMXXZYY series) after different stages of preparation.

nanocomposite samples (TMXXZYY series) exhibited an average roughness around 40 nm regardless of their compositions of nanoparticles. The surface roughness of the nanocomposite was significantly increased after the oxygen plasma treatment. The amount of increase was lower for the nanocomposites containing a higher ratio of small size of ~25 nm M-silica (TM40Z10 and TM50Z00) as compared to the nanocomposites containing an equal or higher ratio of large size of ~100 nm Z-silica (TM25Z25, TM40Z10, and TM50Z00). The results can be rationalized as the following. On the same weight base, the number of small-size particles is higher than the number of large-size particles. Thus, at the same content of mix-size silica nanoparticles in the nanocomposite, the number of nanoparticles will be increased with increasing small-size nanoparticles, which greatly increases the amount of interfaces and reduces the distance between nanoparticles. The increased organic–inorganic hybrid interfaces would retard the deeper etching by the plasma. The surface roughness of the nanocomposite was slightly increased further after the dip-coating which may come from the shrinkage of the nanocomposite with subsequent heat treatment. After the coating of fluorosilane, the nanocomposites of TM10Z40 and TM25Z25 exhibited an average roughness above 100 nm because they have a higher content of ~100 nm Z-silica.

The surface morphology of fluorosilane-coated samples (F-TMXXZYY series) was studied by SEM as shown in Figure 6. The undulated surface of nanosized hills and basins was clearly observed for the F-TM00Z50 sample because it contained only large-size Z-silica (Figure 6(a)). The basins were made of a plasma-etched organic matrix, and the hills were made of plasma-resistant silica nanoparticles. The submicrometer hills and basins made little contribution to the surface roughness of the nanocomposite. By substituting small-size M-silica (~ 25 nm) for 20 wt % of large-size Z-silica (F-TM10Z40 sample), both the area and the number of the basins on the surface were increased (Figure 6(b)). Initially, the small-size M-silica naturally tended to aggregate and attached onto Z-silica which resulted in less protection for the polyacrylate matrix. Thus, both etching area and depth were increased. When the amount of small-size M-silica increased further as the total amount of SiO_2 was kept at 50 wt %, the increased organic–inorganic interfaces reduced the etching depth of the

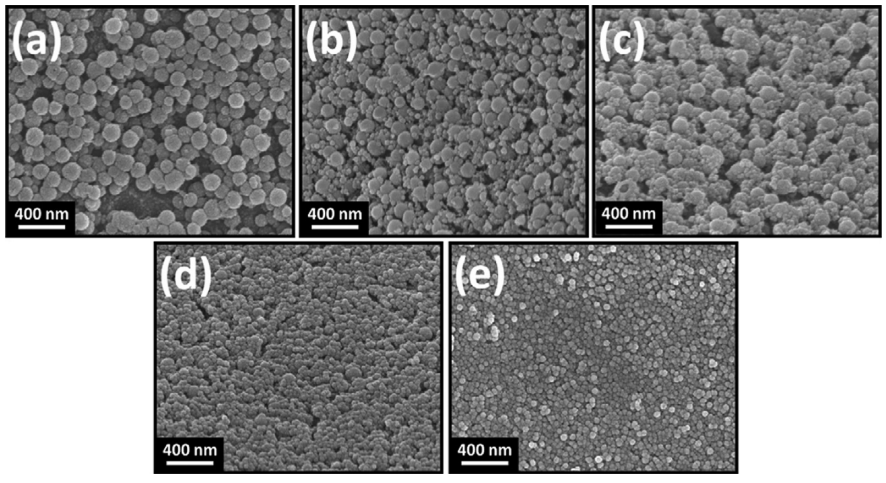

Figure 6. SEM top-view images of various nanocomposites after oxygen plasma and fluorosilane coating. (a) F-TM00Z50, (b) F-TM10Z40, (c) F-TM25Z25, (d) F-TM40Z10, and (e) F-TM50Z00.

Table 2. Water and *n*-1-Octadecene Contact Angles of TMXXZYY Series Nanocomposites after Different Stages of Preparation

	water contact angle (degree)			*n*-1-octadecene contact angle (degree)		
sample name	untreated	O_2 plasma treatment	PFDTMES coating	untreated	O_2 plasma treatment	PFDTMES coating
TM00Z50	104.3 ± 2.5	<1	143.5 ± 4.1	8.9 ± 1.7	<1	101.7 ± 4.1
TM10Z40	104.1 ± 1.7	<1	158.2 ± 3.5	8.5 ± 2.4	<1	128.5 ± 3.3
TM25Z25	105.6 ± 1.9	<1	149.1 ± 3.7	9.8 ± 1.9	<1	112.8 ± 3.7
TM40Z10	104.7 ± 1.5	<1	137.4 ± 2.8	6.1 ± 3.7	<1	81.5 ± 2.3
TM50Z00	103.9 ± 2.1	<1	135.8 ± 3.2	10.1 ± 1.5	<1	80.9 ± 3.6
TCDDA	95.7 ± 1.2	<1	–	8.7 ± 3.2	<1	–

polyacrylate matrix. As a result, the surface roughness was decreased. This observation is consistent with the results of roughness study; the increase in extent of roughness is less in the nanocomposites containing higher content of M-silica (TM40Z10 and TM50Z00) after plasma treatment as discussed above.

3.3. Dewetting Properties of the Nanocomposite. The water and *n*-1-octadecene contact angles of the nanocomposite after different stages of preparation are listed in Table 2. The TM10Z40 nanocomposite exhibited the best omniphobic property after the oxygen plasma treatment and fluorosilane coating. Figure 7 shows the change of water and *n*-1-octadecene contact angles, respectively, on the surface of the TM10Z40 nanocomposite after different surface treatments.

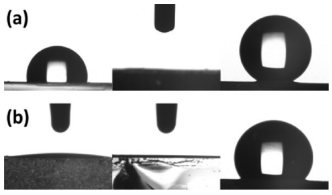

Figure 7. Change of contact angles of (a) water and (b) *n*-1-octadecene on the surface of the TM10Z40 nanocomposite surface after different stages of preparation; image from left to right, as cast, oxygen plasma treatment, and F-silane coating.

All surfaces of pristine nanocomposites had a water contact angle of ∼103° due to the hydrophobicity of the poly(tricyclodecane dimethanol diacrylate) and roughness induced by the process of film casting. After their surfaces were treated by oxygen plasma, the contact angle of each sample was decreased to below 1°. This result may come from the formation of hydrophilic and polar carbonyl, carboxyl, and hydroxyl groups by oxygen plasma and the exposure of hydrophilic silica surfaces.[29] The surface tension was decreased due to the increased polarity on the surface, which was also the cause for this superhydrophilicity. After the dip-coating of fluorosilane on the plasma-treated nanocomposite, the water contact angles of all samples were increased above 130°. The samples of F-TM10Z40 and F-TM25Z25 exhibited superhydrophobic characteristics with contact angles of 158.2° and 149.1°, respectively, which were due to the combination of the roughened surface and the fluorosilane coating.

In the study of the *n*-1-octadecene contact angle on the surface of different nanocomposites, all the surfaces of pristine nanocomposites exhibited a contact angle around 10° due to the oleophilicity of the poly(tricyclodecane dimethanol diacrylate), which had a contact angle less than 10°. The contact angle was decreased below 1° after the oxygen plasma treatment on the nanocomposite (Table 2) because of the increased surface roughness. Although the surface became more polar after the treatment, the interfacial surface energy was increased from the increased surface roughness which was able to overcome the van der Waals force of *n*-1-octadecene. Thus, the contact angle of n-1-octadecene was decreased after plasma treatment. Zimmermann et al. observed a similar phenomenon in their work.[30] However, by dip-coating of fluorosilane on the oxygen plasma treated nanocomposite, the nanocomposite became oleophobic. The nanocomposite of F-TM10Z40 exhibited the highest oleophobicity with an *n*-1-octadecene contact angle of 128.5° among all the samples. This again confirmed the creation of omniphobic structure by the combination of high surface roughness and the fluorosilane coating. Besides, all the other samples also exhibited oleophobic property with contact angles higher than 80°. The *n*-1-octadecene contact angle of the sample was increased with increasing surface roughness which was similar to the results of the water contact angle study discussed before.

To study the connection between the dewetting property and the surface roughness, we measured the advancing and receding contact angles of nanocomposites. For the purposes of comparison, the reference sample fluorosilane coated glass (PFDTMES-glass) was prepared on the flat glass substrate by the same dip-coating process. The results were summarized in Table 3. The average roughness (R_a) of nanocomposites was also listed in the right column of the table. A significant increase in water-advancing contact angles was observed on the

Table 3. Advancing and Receding Contact Angles and Average Roughness of Various Nanocomposites

	contact angle (degree)				
	water		*n*-1-octadecene		
sample name	advancing	receding	advancing	receding	R_a (nm)
F-TM00Z50	143.5 ± 4.1	133.7 ± 3.2	101.7 ± 4.1	92.3 ± 3.7	88.0 ± 5.3
F-TM10Z40	158.2 ± 3.5	147.5 ± 3.7	128.5 ± 3.3	114.5 ± 3.8	126.6 ± 6.1
F-TM25Z25	149.1 ± 3.7	137.3 ± 2.4	112.8 ± 3.7	101.7 ± 4.4	105.5 ± 5.7.
F-TM40Z10	137.4 ± 2.8	121.6 ± 3.1	81.5 ± 2.3	61.2 ± 3.7	68.9 ± 3.8
F-TM50Z00	135.8 ± 3.2	122.4 ± 2.7	80.9 ± 3.6	63.5 ± 2.9	69.4 ± 5.1
PFDTMES-glass	113.5 ± 2.1	110.1 ± 2.3	59.3 ± 2.4	57.8 ± 1.9	7.4 ± 3.3

dx.doi.org/10.1021/am302446t | ACS Appl. Mater. Interfaces 2013, 5, 2991−2998

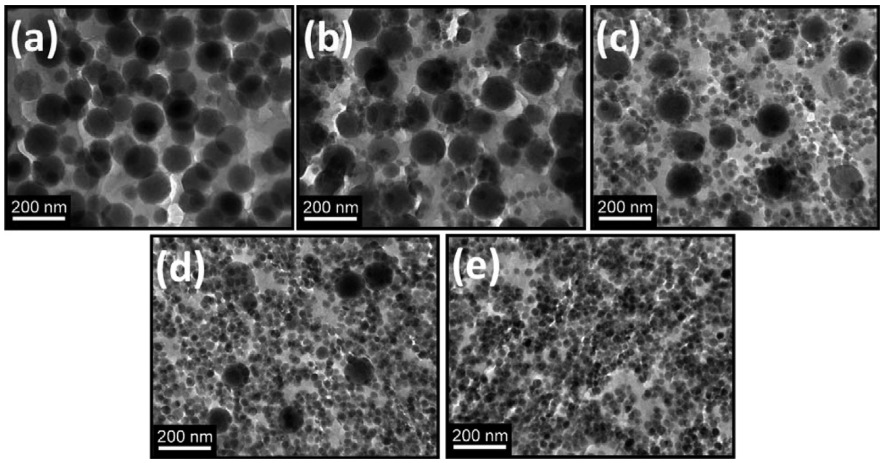

Figure 8. TEM images of the morphology of various nanocomposites: (a) TM00Z50, (b) TM10Z40, (c) TM25Z25, (d) TM40Z10, and (e) TM50Z00.

fluorosilane-coated nanocomposite samples (F-TMXXZYY) as compared with the contact angle of the fluorosilane-coated glass, which resulted from the increased roughness of the nanocomposites after oxygen plasma treatment. However, the superhydrophobicity was only observed in the nanocomposites having R_a above 100 nm. Those nanocomposites contained an equal or larger than 50:50 weight ratio of large-size silica over small-size silica, such as F-TM10Z40 and F-TM25Z25. This roughness value was in agreement with the literature reported results.[4] Both advancing and receding contact angles were increased as the roughness increased, which resulted in a contact angle hysteresis less than 15°. The small hysteresis indicated that the hydrophobicity of fluorosilane-coated nanocomposite was in a state roughly similar to the Cassie–Baxter state of stable hydrophobicity.[13]

In the *n*-1-octadecene contact angle examination, the advancing contact angles of F-TM00Z50, F-TM10Z40, and F-TM25Z25 were higher than 100° even though the contact angle of the fluorosilane-coated glass reference was about 60°. According to the work of Tuteja et al., this phenomenon may correspond to a metastable Cassie–Baxter state.[5] However, a totally wetting stage did not happen even though the volume of the droplet was increased to about 10 μL, which was in contrast to the proposed metastable Cassie–Baxter state. As shown in Figure 6(a)–(c), structures of hills and basins were formed by the aggregation of the silica nanoparticle and the etching of oxygen plasma. When the volume of the *n*-1-octadecene drop was increased, the liquid may only penetrate into some of the basins. The air pockets in the remaining basins and the small-sized valleys prevented a totally wetted stage. Thus, a large contact angle hysteresis was not observed. The results indicated the stable oleophobicity was achieved for the nanocomposites containing a high amount of large-size silica (≥50/50 wt ratio of Z-silica to M-silica). For those samples containing a high amount of small-size silica (F-TM40Z10 and F-TM50Z00), their receding contact angles were similar to the contact angle of flat reference, which led to a larger hysteresis as compared with the hysteresis of the other three samples containing a high amount of large-size silica and a rough surface. The large hysteresis indicated that the oleophobicity of F-TM40Z10 and F-TM50Z00 was in a state similar to that of the Wenzel model. In a short summary, the nanocomposites containing a high amount of large-size silica (≥50/50 wt ratio of Z-silica to M-silica) can exhibit very stable omniphobicity due to the formation of re-entrant structure.[5,6]

3.4. Physical and Chemical Properties of the Nanocomposites. The morphology of the nanocomposites was investigated by TEM. Figure 8 shows the TEM images of nanocomposites with different size nanoparticles. The nanocomposite containing only large-size Z-silica (F-TM00Z50) exhibited a very homogeneous dispersion of nanoparticles in the polymer matrix (Figure 8(a)). By replacing the Z-silica with small-size M-silica in the nanocomposite, the M-silica tended to aggregate around Z-silica that roughened the surface as shown in the samples of F-TM10Z40 (Figure 8(b)) and F-TM25Z25 (Figure 8(c)). When the amount of M-silica was higher than 25 wt % of total silica in nanocomposites (i.e., the ratio of M-silica to Z-silica is >50/50 by wt), the amount of M-silica aggregation was increased as shown in the samples of F-TM40Z10 (Figure 8(d)) and F-TM50Z00 (Figure 8(e)). Besides, Z-silica nanoparticles in the F-TM40Z10 nanocomposite were embedded in the aggregates of M-silica, which contributed to the similar roughness as F-TM50Z00. The influence of aggregation on the physical and chemical properties of nanocomposites is discussed below.

Figure 9(a) shows the nanocomposite exhibited the best optical transmittance when it contained only the small-size M-silica (TM50Z00) due to the least amount of light scattering in the sample. The transmittance was decreased for the nanocomposite made from large-size Z-silica only (TM00Z50) because there was more volume of the organic matrix and a larger difference of the refractive index in TM00Z50 than that of TM50Z00. The transmittance of the nanocomposite was decreased further when it contained mixed size silica due to the formation of aggregates. The extent of aggregation of the nanocomposite became the highest when the silica content was made from the equal weight ratio of small-size silica to large silica such as sample F-TM25Z25. That resulted in the largest scattering and lowest transmittance, especially in the wavelength range shorter than 600 nm. Nevertheless, all the ∼60 μm film samples still exhibited good transparency of 80% at 600 nm wavelength or above. The best omniphobic nanocomposite of TM10Z40 exhibited high transparency (>82% at 450–800 nm). Figure 9(b) and 9(c) show the water vapor permeation rate (WVTR) and water absorption (WA) of F-TMXXZYY series, respectively. Both WVTR and WA were increased as the weight percentage of the small-sized silica nanoparticle was

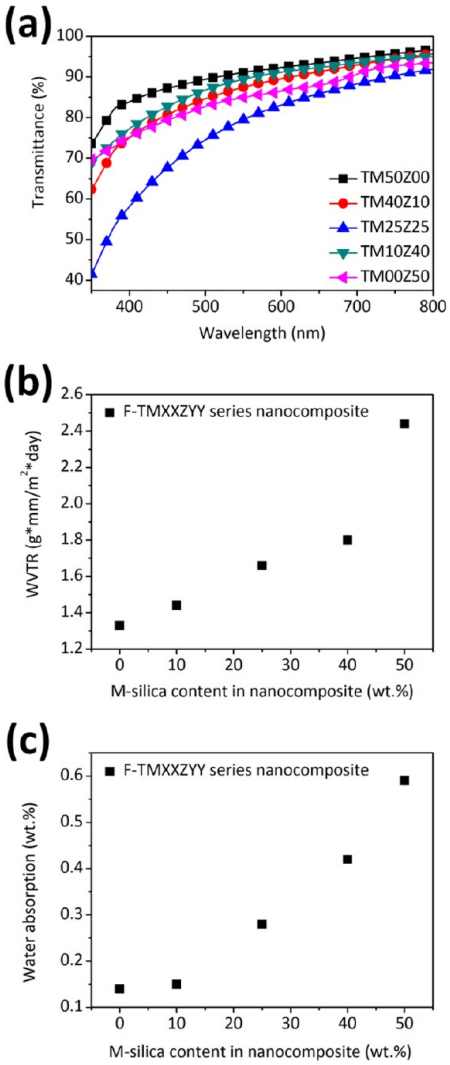

Figure 9. Physical and chemical properties of various nanocomposites at different concentration of M-silica: (a) UV−visible spectrum of ∼60 μm film, (b) water vapor permeation rate, and (c) water absorption.

increased in the nanocomposite. Although the surface of silica was modified by organosilane MPS to be compatible with the organic matrix of the nanocomposite, the modified silica was still relatively hydrophilic due to the presence of the polar carbonyl group of MPS and the residual silanol group of silica.

As discussed before, when the nanocomposite contains the same total silica amount like at 50 wt %, the total number of silica will be determined by the composition of small-size M-silica and large-size Z-silica. The number will be increased faster by increasing the amount of small-size M-silica in the silica composition. Then, the number of both hydrophilic functional groups increases when the content of M-silica increases. The increase of hydrophilic characteristics on the surface facilitates the transport of water molecules into the nanocomposite, even though the water absorption and the WVTR of the nanocomposites were increased when the amount of small M-silica was increased in the nanocomposite. The nanocomposite of TM50Z00 containing all small-size M-silica at 50 wt % (TM50Z00) still exhibited greatly reduced water absorption by 44.34% and WVTR by 79.70% as compared with neat poly(tricyclodecane dimethanol diacrylate) due to the dense characteristic of silica.

The best nanocomposite of F-TM10Z40, when it was a cast film of ∼60 μm thick on a 1 mm glass slide, was clear and transparent as shown in Figure 10. The film can see through the substrate and observe the message (8 pt. characters) underneath. By placing about 2−10 μL of either water (Figure 10(a)) or *n*-1-octadecene (Figure 10(b)) droplets on the surface of the film, an omniphobic characteristic is clearly revealed.

4. CONCLUSIONS

We have successfully developed a novel dense omniphobic nanocomposite with 158.2° water contact angle and 128.5° *n*-1-octadecene contact angle, high transparency (>82% transmittance at 450−800 nm), and low moisture permeation (1.44 g·mm/m^2·day) via a three-step process. First, the mixture of acrylate-modified small and large nanosized silica was dispersed into the acrylate matrix to make UV-cured hybrid nanocomposites, and then the surface of the hybrid was treated with oxygen plasma. Finally, the surface was coated with fluorosilane (PFDTMES). The oxygen plasma is a useful process for roughening the surface and exposing silica nanoparticles to create a nanotexture surface, and then the exposed silica can be further reacted with fluorosilane to obtain a low surface tension surface. The outstanding physical and chemical property of this new omniphobic nanocomposite can find potential applications in the encapsulation of optoelectronics, self-cleaning coatings, etc.

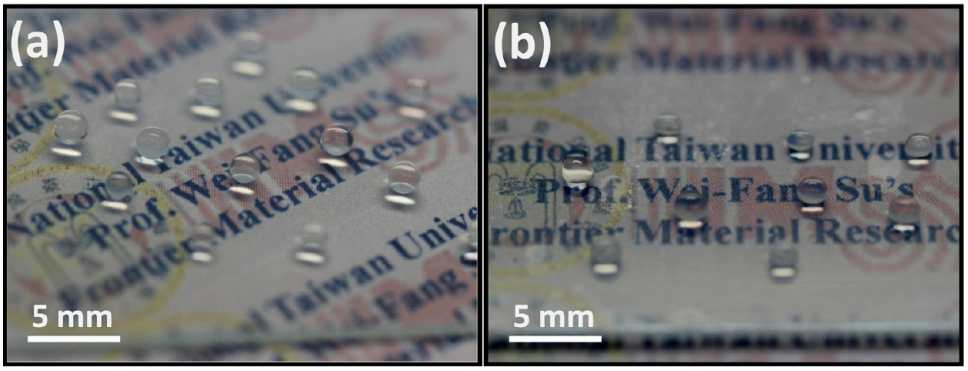

Figure 10. Photos of 60 μm film of the F-TM10Z40 nanocomposite on a 1 mm glass slide with liquid droplets on the surface: (a) water and (b) *n*-1-octadecene. The volume of droplets is around 2−6 μL. (Logo on the left of the figure was used by permission of National Taiwan University.)

dx.doi.org/10.1021/am302446t | ACS Appl. Mater. Interfaces 2013, 5, 2991−2998

AUTHOR INFORMATION

Corresponding Author

*E-mail: suwf@ntu.edu.tw.

Notes

The authors declare no competing financial interest.

ACKNOWLEDGMENTS

The financial support obtained from the National Science Council of Taiwan to carry out this research is highly appreciated (NSC 101-2120-M-002-003 and NSC100-3113-E-00 2-012).

REFERENCES

(1) Barthlott, W.; Neinhuis, C. *Planta* **1997**, *202*, 1−8.
(2) Wagner, T.; Neinhuis, C.; Barthlott, W. *Acta Zool.* **1996**, *77*, 213−225.
(3) Gao, X. F.; Jiang, L. *Nature* **2004**, *432*, 36−36.
(4) Neumann, A. W.; Good, R. J. *J. Colloid Interface Sci.* **1972**, *38*, 341−358.
(5) Tuteja, A.; Choi, W.; Ma, M.; Mabry, J. M.; Mazzella, S. A.; Rutledge, G. C.; McKinley, G. H.; Cohen, R. E. *Science* **2007**, *318*, 1618−1622.
(6) Tuteja, A.; Choi, W.; Mabry, J. M.; McKinley, G. H.; Cohen, R. E. *Proc. Natl. Acad. Sci. U.S.A.* **2008**, *105*, 18200−18205.
(7) Boreyko, J. B.; Baker, C. H.; Poley, C. R.; Chen, C. H. *Langmuir* **2011**, *27*, 7502−7509.
(8) Nakajima, A.; Hashimoto, K.; Watanabe, T.; Takai, K.; Yamauchi, G.; Fujishima, A. *Langmuir* **2000**, *16*, 7044−7047.
(9) Joly, L.; Biben, T. *Soft Matter* **2009**, *5*, 2549−2557.
(10) Vilčnik, A.; Jerman, I.; Vuk, A. Š.; Koželj, M.; Orel, B.; Tomšič, B.; Simončič, B.; Kovač, J. *Langmuir* **2009**, *25*, 5869−5880.
(11) Xu, Q. F.; Wang, J. N.; Sanderson, K. D. *ACS Nano* **2010**, *4*, 2201−2209.
(12) Meuler, A. J.; Smith, J. D.; Varanasi, K. K.; Mabry, J. M.; McKiney, G. H.; Cohen, R. E. *ACS Appl. Mater. Interfaces* **2010**, *2*, 3100−3110.
(13) Cassie, A. B. D.; Baxter, S. *Trans. Faraday Soc.* **1944**, *40*, 546−550.
(14) Wenzel, R. N. *Ind. Eng. Chem.* **1936**, *28*, 988−994.
(15) Tsougeni, K.; Vourdas, N.; Tserepi, A.; Gogolides, E.; Cardinaud, C. *Langmuir* **2009**, *25*, 11748−11759.
(16) Bravo, J.; Zhai, L.; Wu, Z.; Cohen, R. E.; Rubner, M. F. *Langmuir* **2007**, *23*, 7293−7298.
(17) Xu, Q. F.; Wang, J. N.; Smith, I. H.; Sanderson, K. D. *J. Mater. Chem.* **2009**, *19*, 655−660.
(18) Ling, X. Y.; Phang, I. Y.; Vancso, G. J.; Huskens, J.; Reinhoudt, D. N. *Langmuir* **2009**, *25*, 3260−3263.
(19) Cao, L.; Gao, D. *Faraday Discuss.* **2010**, *146*, 57−65.
(20) Im, M.; Im, H.; Lee, J.-H.; Yoon, J.-B.; Choi, Y.-K. *Soft Matter* **2010**, *6*, 1401−1404.
(21) Zhai, L.; Cebeci, F. C.; Cohen, R. E.; Rubner, M. F. *Nano Lett.* **2004**, *4*, 1349−1353.
(22) Iacono, S. T.; Budy, S. M.; Smith, D. W., Jr.; Mabry, J. M. *J. Mater. Chem.* **2010**, *20*, 2979−2984.
(23) Meng, L. Y.; Park, S. J. *J. Colloid Interface Sci.* **2010**, *342*, 559−563.
(24) Vandencasteele, N.; Nisol, B.; Viville, P.; Lazzaroni, R.; Castner, D. G.; Reniers, F. *Plasma Process. Polym.* **2008**, *5*, 661−671.
(25) Lin, C. C.; Hsu, S. H.; Chang, Y. L.; Su, W. F. *J. Mater. Chem.* **2010**, *20*, 3084−3091.
(26) Lin, C. C.; Chang, K. H.; Lin, K. C.; Su, W. F. *Compos. Sci. Technol.* **2009**, *69*, 1180−1186.
(27) Luscombe, C. K.; Li, H. W.; Huck, W. T. S.; Holmes, A. B. *Langmuir* **2003**, *19*, 5273−5278.
(28) Ulman, A. *Chem. Rev.* **1996**, *96*, 1533−1554.
(29) Sanchis, M. R.; Blanes, V.; Blanes, M.; Garcia, D.; Balart, R. *Eur. Polym. J.* **2006**, *42*, 1558−1568.
(30) Zimmermann, J.; Rabe, M.; Artus, G. R. J.; Seeger, S. *Soft Matter* **2008**, *4*, 450−452.